Large Improvement in Image Rejection of Double-Quadrature Dual-Conversion Low-IF Architectures

Jin-Siang Syu, *Student Member, IEEE*, Chin-Chun Meng, *Member, IEEE*, Ya-Hui Teng, and Hua-Yu Liao

***Abstract*—The reasons for a degradation of image-rejection performance in double-quadrature–double-quadrature and single-quadrature–double-quadrature dual-conversion low-IF downconverters are fully discussed in this paper. Polyphase filters (PPFs) are inserted at proper positions to minimize the effects of device/signal mismatches, and thus improve the image rejection without calibration. Both a 0.35-μm SiGe heterojunction bipolar transistor 5.2-GHz double-quadrature–double-quadrature downconverter with an RF PPF and a 0.18-μm CMOS 2.2/4.8-GHz single-quadrature–double-quadrature downconverter with a switched-band low-noise amplifier (LNA) and a narrowband inter-stage PPF are demonstrated. Compared with our previous work, the 5.2-GHz downconverter achieves a 15-dB improvement in image-rejection ratio (IRR) of the first image signal (IRR_1) even without a pre-selection filter or LNA. Additionally, the dual-band downconverter has a 25-dB improvement in IRR of the second image signal (IRR_2), which nearly reaches the theoretical limit of a four-stage PPF covering 20–40 MHz.**

***Index Terms*—Dual conversion, Hartley architecture, image rejection, low IF, polyphase filter (PPF), Weaver architecture.**

I. Introduction

A LOW-IF down-conversion architecture is widely used [1]–[3] since this architecture can eliminate dc offset and flicker noise problems. A static or random dc offset may cause a demodulation error while preposterous $1/f$ noise may cover up desired signals and results in a fatal detection error, especially in a CMOS process [4]–[6]. On the other hand, series capacitors can be added at the output to block the dc component in a low-IF receiver because the down-converted signal is not located at dc. The $1/f$ noise can be avoided by choosing a proper IF band beyond the $1/f$ noise corner. However, a higher IF band results in higher power consumption for the subsequent analog-to-digital converter (ADC). Besides, a dual-conversion downconverter alleviates the burden of a high-frequency local oscillator (LO) signal generation, but two conversions have two image bands to be suppressed.

In previous literature of dual-conversion low-IF downconverters [7]–[10], including our previous work, the IRR_1 was limited to about 40–45 dB without a low-noise amplifier (LNA); while the IRR_2 was unable to reach the theoretical limit due to device/signal mismatch, layout path imbalance, and process variations. In this paper, two Weaver–Hartley dual-conversion low-IF downconverters are demonstrated with large improvement in image rejection. A Weaver architecture [11], [12] is a complex dual-conversion system, while a Hartley architecture [13] consists of a complex mixer and a complex filter such as a passive microwave coupler [14], a polyphase filter (PPF) [9], [15] or an active complex bandpass filter [3], [16], [17]. In this paper, a 5.2-GHz double-quadrature–double-quadrature downconverter, using a preceding RF PPF achieves a high IRR_1 at the cost of noise performance and power consumption. Additionally, a 2.2/4.8-GHz dual-band single-quadrature–double-quadrature receiver employs a switched-band LNA to pre-filter the first image signal. An inter-stage PPF, employed between the first- and second-stage mixers, also achieves significant improvement in the quadrature accuracy of output in-phase/quadrature (I/Q) signals and also the IRR_2.

This paper is organized as follows. Single-band/multiband quadrature signal generators are introduced in Section II, while Section III reviews the Weaver–Hartley hybrid architectures with emphasis on nonideal effects. Circuit implementations and measurement results of a single-band double-quadrature–double-quadrature Weaver–Hartley downconverter and a dual-band single-quadrature–double-quadrature Weaver–Hartley downconverter are reported in Section IV. Conclusions are outlined in Section V, and finally, a dual-band double-quadrature–double-quadrature Weaver–Hartley architecture is also proposed at the end of this paper for further improvement in image-rejection ratio (IRR).

II. Quadrature Signal Generation

A. Phasor and Complex Representations for Real Signals

A phasor ($\vec{v} = Ae^{j\theta}$) includes the information of amplitude (A) and phase (θ) of a real signal. An arbitrary phasor sequence (four vectors) can be decomposed into four balanced sequences [15], [18], which are: 1) quadrature counterclockwise (right-

Manuscript received October 27, 2009; revised March 19, 2010; accepted April 08, 2010. Date of publication May 24, 2010; date of current version July 14, 2010. This work was supported by the National Science Council of Taiwan under Contract NSC 98-2221-E-009-033-MY3, Contract NSC 98-2221-E-009-031, and Contract NSC 98-2218-E-009-008-MY3, by the Ministry of Economic Affairs of Taiwan under Contract 96-EC-17-A-05-S1-020, and by the Ministry of Education (MoE) Aim for the Top University (ATU) Program under Contract 95W803.

The authors are with the Department of Electrical Engineering, National Chiao Tung University, Hsinchu 300, Taiwan (e-mail: jssyu.cm95g@nctu.edu.tw; fifiya.cm95g@nctu.edu.tw; hy_liao.cm93g@nctu.edu.tw; ccmeng@mail.nctu.edu.tw).

Color versions of one or more of the figures in this paper are available online at http://ieeexplore.ieee.org.

Digital Object Identifier 10.1109/TMTT.2010.2049695

0018-9480/$26.00 © 2010 IEEE

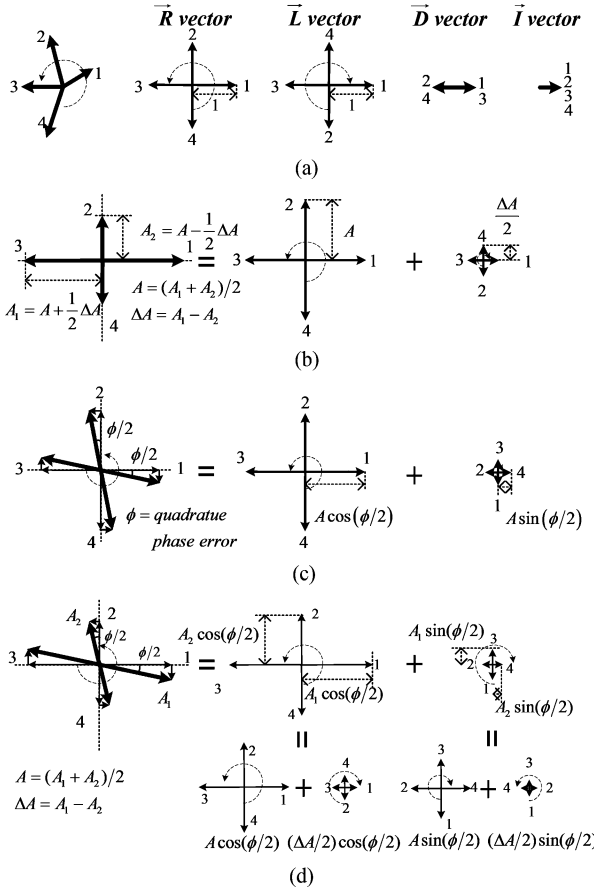

Fig. 1. (a) Balanced phasor sets $\vec{R}$, $\vec{L}$, and $\vec{I}$. (b) Phasor set with amplitude imbalance (ΔA). (c) Phasor set with quadrature phase error (ϕ). (d) Phasor set with both phase and amplitude imbalance.

handed) sequence $\vec{R}$; 2) quadrature clockwise (left-handed) sequence $\vec{L}$; 3) collinear differential sequence $\vec{D}$; and 4) collinear in-phase sequence $\vec{I}$, as indicated in Fig. 1(a). A differential amplitude/phase imbalance affects the isolation and second-order nonlinearity significantly, but not gain and image rejection [15]. Therefore, assuming a phasor sequence is fully differential for simplicity, the phasor sequence is simply a linear combination of a right-handed sequence $\vec{R}$ and a left-handed sequence $\vec{L}$. The right-handed sequence $\vec{R}(0°, 90°, 180°, 270°)$ can be denoted as a complex signal $\exp(j\omega t)$, while the left-handed sequence $\vec{L}(0°, 270°, 180°, 90°)$ represents $\exp(-j\omega t)$ [12]. In addition, an error function (ε) is defined as an amplitude ratio of $\vec{L}$ and $\vec{R}$ to facilitate the analysis throughout this paper. Since a down-converted image signal is at the opposite spectrum of a desired signal, the reciprocal of the error function is equal to the IRR.

For example, a phasor sequence with unbalanced amplitudes $(A_1 = A + \Delta A/2(b)$ and $A_2 = A - \Delta A/2)$, as shown in Fig. 1(b), can be decomposed into

$$\vec{V} = A\vec{R} + \frac{\Delta A}{2}\vec{L} \tag{1}$$

with an error function

$$\varepsilon_r = \left|\frac{\Delta A}{(2A)}\right| = \left|\frac{(A_1 - A_2)}{(A_1 + A_2)}\right|. \tag{2}$$

Similarly, a phasor sequence with a balanced amplitude (A), but a quadrature phase error (ϕ), as shown in Fig. 1(c), can be decomposed into

$$\vec{V} = A\cos\left(\frac{\phi}{2}\right)\vec{R} - jA\sin\left(\frac{\phi}{2}\right)\vec{L}. \tag{3}$$

with an error function

$$\varepsilon_\phi = \left|\tan\left(\frac{\phi}{2}\right)\right|. \tag{4}$$

Generally, a phasor sequence with both amplitude imbalance and phase error, as shown in Fig. 1(d), can be decomposed into

$$\vec{V} = \left[\cos\left(\frac{\phi}{2}\right)A - j\sin\left(\frac{\phi}{2}\right)\left(\frac{\Delta A}{2}\right)\right]\vec{R} + \left[\cos\left(\frac{\phi}{2}\right)\left(\frac{\Delta A}{2}\right) - j\sin\left(\frac{\phi}{2}\right)A\right]\vec{L}. \tag{5}$$

Hence, an overall error function becomes

$$\varepsilon_{r,\phi} = \left|\frac{\varepsilon_r - j\varepsilon_\phi}{1 - j\varepsilon_\phi\varepsilon_r}\right| = \sqrt{\frac{\varepsilon_r^2 + \varepsilon_\phi^2}{1 + \varepsilon_r^2\varepsilon_\phi^2}}. \tag{6}$$

It is evident that either a phase error or an amplitude imbalance produces an opposite phasor sequence. It is worthwhile to mention that the reciprocal of calculated results is the IRR in an image-rejection receiver described in [19, eq. (5.15)] with LO quadrature amplitude/phase mismatches

$$\mathrm{IRR} = \frac{A_1^2 + 2A_1A_2\cos\phi + A_2^2}{A_1^2 - 2A_1A_2\cos\phi + A_2^2} \tag{7}$$

where $(A_1^2 + A_2^2) = 2A^2(1 + \varepsilon_r^2)$, $2A_1A_2 = 2A^2(1 - \varepsilon_r^2)$, and $\cos\phi = (1 - \varepsilon_\phi^2)/(1 + \varepsilon_\phi^2)$.

B. Lumped Quadrature Signal Generation Methods

A distributed microwave quadrature coupler, such as a quarter-wavelength coupled-line coupler, a Lange coupler, or a branch-line coupler, occupies enormous die area, especially for low-frequency applications (e.g., below 10 GHz). Instead of microwave realizations, lumped quadrature signal generators are widely used at low frequencies. An RC–CR PPF is one of the widely used solutions. The transfer function of a single-stage PPF [see Fig. 2(a)] with a balanced quadrature phasor sequence ($\vec{R}$ or $\vec{L}$) is expressed as

$$A_{Vo\pm}(\omega) = \frac{1 \pm \frac{\omega}{\omega_0}}{1 + j(\frac{\omega}{\omega_0})} \tag{8}$$

where $\omega_0 = 1/RC$ is the transmission zero of A_{Vo-} and also the pole frequency of both A_{Vo+} and A_{Vo-}.

Thus, the equivalent error function is defined as

$$\varepsilon_0(\omega) \equiv \left|\frac{A_{Vo-}}{A_{Vo+}}\right| = \left|\frac{\omega - \omega_0}{\omega + \omega_0}\right|. \tag{9}$$

For a quadrature signal generation, the input differential signal can be decomposed into $\vec{R}$ and $\vec{L}$ with the same amplitudes; thus, the output error function has the same meaning as the ratio of negative and positive signal gain, defined in (9).

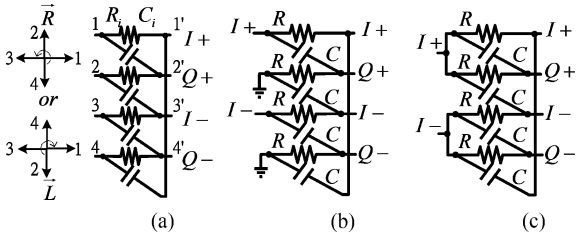

Fig. 2. (a) Single-stage PPF with a balanced quadrature phasor input ($\vec{R}$ or $\vec{L}$). (b) PPF with Q input shorted to ground. (c) PPF with I/Q input connected together.

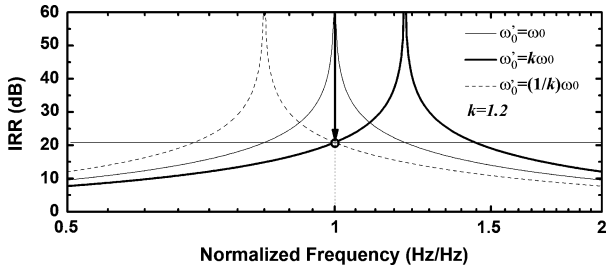

Fig. 3. IRR with a pole frequency deviation due to a process variation.

A single-stage PPF with Q input shorted to the ground, as shown in Fig. 2(b), has a quadrature output ratio

$$\frac{Q(\omega)}{I(\omega)} = j\frac{\omega}{\omega_0} = \left|\frac{\omega}{\omega_0}\right| e^{j90^\circ}. \tag{10}$$

The output phasor sequence belongs to a constant-quadrature-phase sequence, illustrated in Fig. 1(b); thus, by (2), the error function becomes

$$\varepsilon_0(\omega) = \left|\frac{\Delta A}{2A}\right| = \left|\frac{|Q|-|I|}{|Q|+|I|}\right| = \left|\frac{\omega-\omega_0}{\omega+\omega_0}\right| \tag{11}$$

where $\omega_0 = 1/RC$.

On the other hand, a PPF with I/Q input connected, as shown in Fig. 2(c), has a quadrature output ratio of

$$\frac{Q(\omega)}{I(\omega)} = \frac{1+sRC}{1-sRC} = \frac{1+j\omega\omega_0}{1-\frac{j\omega}{\omega_0}} = e^{j\left[2\tan^{-1}(\omega/\omega_0)\right]} = e^{j(90^\circ+\phi)} \tag{12}$$

where $\phi/2 = \tan^{-1}(\omega/\omega_0) - 45^\circ$.

Therefore, the output phasor sequence has balanced amplitudes, but a phase error ϕ, the same as Fig. 1(c). By (4), the error function becomes

$$\varepsilon_0(\omega) = \left|\tan\left(\frac{\phi}{2}\right)\right| = \left|\frac{\omega-\omega_0}{\omega+\omega_0}\right|. \tag{13}$$

As analyzed above, even though one topology always has a quadrature phase difference while the other type always has exact balanced amplitudes, the two PPF topologies have the same error function.

Moreover, Fig. 3 shows the correspondent IRR of the PPF ($-20\log|\varepsilon_o|$) with a center frequency variation due to process variation. If a center frequency varies 20%, the IRR is drastically degraded to only 20.8 dB. Therefore, the process variation should be taken into account when deciding a sufficient IRR bandwidth.

C. Wide-Band/Multiband Extensions by Multistage PPF

For a multistage PPF with a balanced quadrature phasor sequence ($\vec{R}$ or $\vec{L}$), the transfer function can be expressed as

$$A_{V\pm}(\omega) = \prod_{i=1}^{N} A_{Voi\pm}(\omega)\frac{Z_{Li}}{Z_{Si}+Z_{Li}} \tag{14}$$

and its correspondent error function can thus be expressed as

$$\varepsilon = \frac{\left[\prod_{i=1}^{N}|A_{Voi-}(\omega)|\right]}{\left[\prod_{i=1}^{N}|A_{Voi+}(\omega)|\right]} = \prod_{i=1}^{N}\left|\frac{\omega-\omega_i}{\omega+\omega_i}\right| \tag{15}$$

where $A_{Voi\pm}(\omega)$ is the open-circuited voltage gain of the i_{th}-stage PPF, defined by (8); Z_{Si}/Z_{Li} is the equivalent source/load impedance of the i_{th} stage.

The A_{Vo+} of each stage is larger than 1 and reaches the maximum value of $\sqrt{2}$ at the center frequency. Thus, the impedance ratio between each stage and the input/output impedance dominate the overall voltage gain/loss. On the other hand, the voltage gain of the A_{Vo-} has a transmission zero and results in a narrowband rejection response.

With different locations of transmission zeros of a multistage PPF, there are three typical circumstances, which are: 1) narrowband ($\omega_{\max}/\omega_{\min}1$); 2) wideband ($\omega_{\max}/\omega_{\min} \gg 1$); and 3) multiband applications.

1) For a narrowband application, all the transmission zeros are identical, ω_0; thus, an N-stage PPF provides a total error of $\varepsilon = \varepsilon_o^N$, thus the error is reduced with increasing cascading stages, as shown in Fig. 4(a). In other words, for a given tolerable IRR ($-20\log|\varepsilon|$), the ratio bandwidth becomes

$$\frac{\omega_{\max}}{\omega_{\min}} = \left(\frac{1+\varepsilon^{1/N}}{1-\varepsilon^{1/N}}\right)^2 = \left(\frac{1+\varepsilon_0}{1-\varepsilon_0}\right)^2 \tag{16}$$

where ε is the target error function after the PPF, ε_o is the error function of one-stage PPF, and N is the number of stages.

Thus, for a target 40-dB IRR ($\varepsilon = 0.01$) of a quadrature generator, the ratio bandwidth becomes 1.041, 1.494, and 2.4 for single-, two-, and three-stage PPFs, respectively.

In addition, the voltage gain (or loss) of a multistage PPF with the same center frequency can be calculated. By (14), the voltage gain of an N-stage PPF at the center frequency can be expressed as

$$\begin{aligned}|A_{Vo+}(\omega_0)| &= \left|\prod_{1}^{n}\frac{1+\frac{\omega}{\omega_0}}{1+j\frac{\omega}{\omega_0}}\prod_{1}^{n}\frac{Z_{(i+1)}}{Z_{(i+1)}+Z_{(i)}}\right| \\ &= 2^{n/2}\prod_{i=1}^{n}\frac{1}{1+\frac{R_{(i)}}{R_{(i+1)}}}\end{aligned} \tag{17}$$

where $Z_{(i)}(\omega_0) = R_i/(1+j) = 1/[\omega_0 C_i(1+j)]$, $\omega_0 = 1/R_iC_i, \forall i \in \{1,2,\ldots,N\}$, and $Z_{N+1} = Z_L = \infty$.

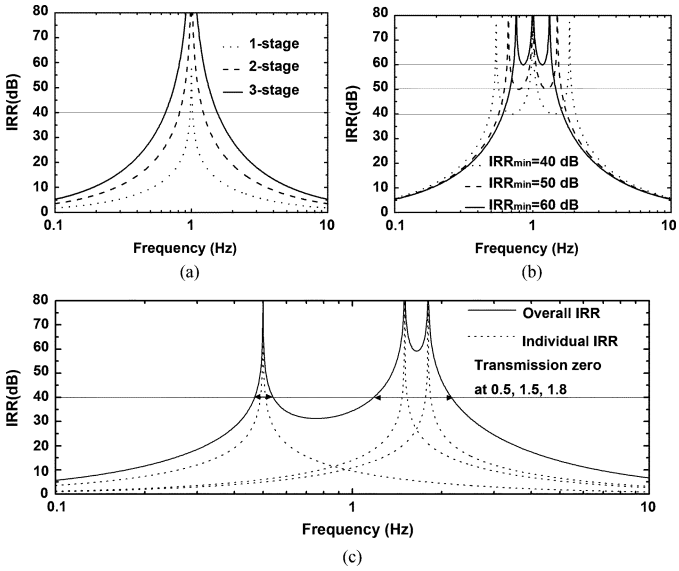

Fig. 4. Three-stage PPF on different pole locations. (a) Equal RC pole. (b) Unequal RC poles with an equiripple frequency response. (c) Unequal RC poles for multiband applications.

Equation (17) shows that the increase of resistance lessens the voltage loss when the last stage is open circuited [15]. However, in reality, the loading of the PPF is the gate (base) of the active mixer core with capacitive impedance of $1/sC_L$. Thus, the input impedance is typically open circuited at low frequencies, but degrades at high frequencies. The voltage gain should be modified as

$$|A_{V+}(\omega_0)| = \left|A_{Vo+}(\omega_0)\frac{Z_L}{Z_N+Z_L}\right| = |A_{Vo+}(\omega_0)|\sqrt{\frac{2}{1+\left(1+\frac{C_L}{C_N}\right)^2}}. \quad (18)$$

Although the increase of resistance can increase A_{Vo+}, the small capacitance at the $N_{\rm th}$ stage (C_N), resulting from a high resistance (R_N), may degrade the overall voltage gain, especially at high frequencies. Thus, an optimum voltage gain always exists if the source impedance (Z_S) and the output loading capacitance (C_L) are given.

2) For a wideband application, a multistage PPF with logarithmic increase of pole locations results in an equiripple image rejection frequency response, as shown in Fig. 4(b). The derivation of optimum pole locations for a minimum IRR of an N-stage PPF had been proposed for a given ratio bandwidth $\omega_{\max}/\omega_{\min}$ [15]. Thus, for a target IRR, the number of stages and the pole locations can be defined [15].

3) Finally, for a multiband quadrature generation, each stage of a PPF is set at different desired frequencies, as shown in Fig. 4(c). The image-rejection bandwidth becomes wider when compared to the individual response because the distant away transmission zeros still provide a certain effect on a given band. Certainly, detailed information on gain and IRR bandwidth can be obtained by simulation tools.

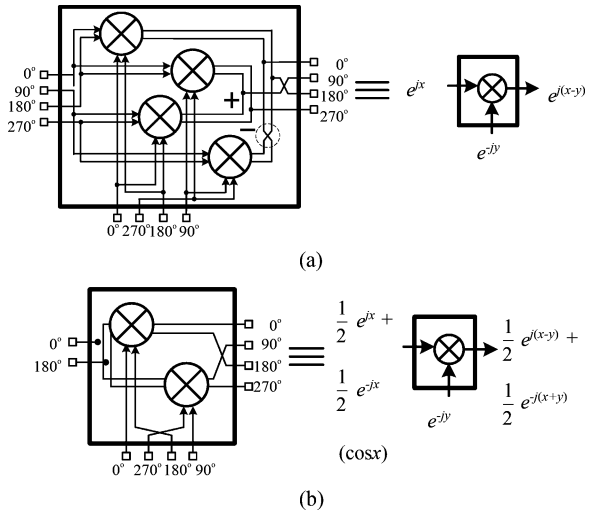

Fig. 5. (a) Schematic of a double-quadrature complex mixer topology and its complex representation. (b) Schematic of a single-quadrature topology and its complex representation.

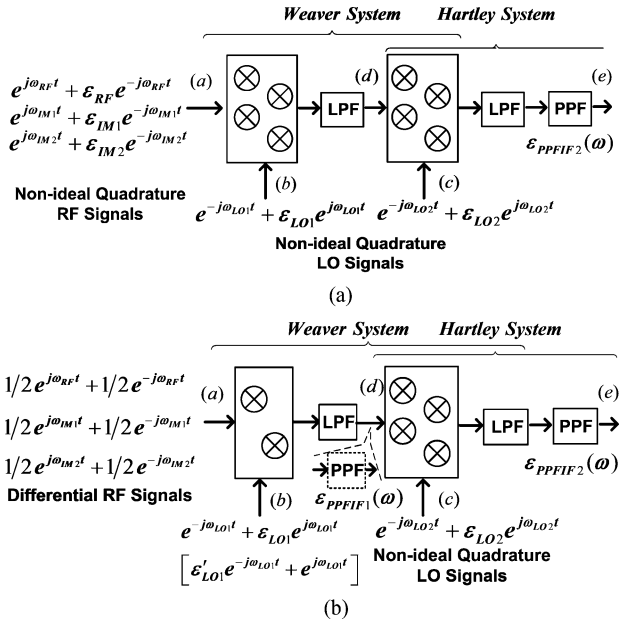

Fig. 6. Block diagrams of a: (a) double-quadrature–double-quadrature dual-conversion system and (b) single-quadrature–double-quadrature dual-conversion system with nonideal input signals.

III. Weaver–Hartley Image-Rejection Architecture

A. Introduction of Weaver–Hartley Architecture

Mixing operations of complex double- and single-quadrature topologies can be expressed by the complex signal multiplication, as shown in Fig. 5(a) and (b), respectively. A double-quadrature mixer topology includes four real mixers with two quadrature inputs, while a single-quadrature complex mixer has two real mixers with only one of the two inputs being quadrature. Double-quadrature–double-quadrature/single-quadrature–double-quadrature Weaver–Hartley architectures and their complex notations are illustrated in Fig. 6(a) and (b), respectively. The desired RF signal and image signals are down-converted to a low-IF band by the first LO

(LO_1) and second LO (LO_2). The angular frequencies of the desired, first image, second image, first LO, and second LO signals are denoted as ω_{RF}, ω_{IM1}, ω_{IM2}, ω_{LO1}, and ω_{LO2}, respectively. Additionally, the angular frequencies of the IF signal after the first and second down-conversions are defined as ω_{IF1} and ω_{IF2}, respectively.

The relations of the signals defined above can be expressed as

$$\begin{cases} \omega_{\mathrm{RF}} - \omega_{\mathrm{LO1}} = \omega_{\mathrm{LO1}} - \omega_{\mathrm{IM1}} = \omega_{\mathrm{IF1}} \\ \omega_{\mathrm{RF}} - (\omega_{\mathrm{LO1}} + \omega_{\mathrm{LO2}}) = (\omega_{\mathrm{LO1}} + \omega_{\mathrm{LO2}}) - \omega_{\mathrm{IM2}} = \omega_{\mathrm{IF2}} \\ \omega_{\mathrm{IF1}} = \omega_{\mathrm{LO2}} + \omega_{\mathrm{IF2}}. \end{cases} \tag{19}$$

The operations of double-quadrature–double-quadrature/single-quadrature–double-quadrature can be well explained by the frequency shifting in the spectrum [12]. Since the quadrature LO_1 signal $\exp(-j\omega_{\mathrm{LO1}}t)$ is located at the negative spectrum, ω_{RF}, ω_{IM1}, and ω_{IM2} signals are first left-shifted to $\omega_{\mathrm{IF1}} - \omega_{\mathrm{IF1}}$, and $\omega_{\mathrm{LO2}} - \omega_{\mathrm{IF2}}$ bands, respectively. Next, signals are down-converted by $\exp(-j\omega_{\mathrm{LO2}}t)$; thus, these signals are left-shifted to ω_{IF2}, $\omega_{\mathrm{IF2}} - 2\omega_{\mathrm{IF1}}$, and $-\omega_{\mathrm{IF2}}$ bands, respectively. After the dual conversions of the Weaver system, the first image signal is shifted out of the output low-pass band. On the other hand, the down-converted second image signal is located at $-\omega_{\mathrm{IF2}}$, which cannot be filtered out by the low-pass filter, but can be highly rejected by the following IF_2 PPF in the Hartley system [10].

For a dual-band application, the polarity of the LO_1 signal is set to be switchable (i.e., the input signal can be chosen to be either left- or right-shifted for a complex mixing) [10]. In order to reuse the second-stage mixers, the LO_1 frequency is set at the halfway point between two application bands. That is, the desired signal of the high-frequency band is the image signal of the low-frequency band and vice versa.

The relations of these signals are given as follows:

$$\begin{cases} \omega_{\mathrm{RFH}}(\omega_{\mathrm{IM1L}}) - \omega_{\mathrm{LO1}} = \omega_{LO1} - \omega_{\mathrm{IM1H}}(\omega_{\mathrm{RFL}}) = \omega_{\mathrm{IF1}} \\ \omega_{\mathrm{RFH}} - (\omega_{\mathrm{LO1}} + \omega_{\mathrm{LO2}}) = (\omega_{\mathrm{LO1}} + \omega_{\mathrm{LO2}}) - \omega_{\mathrm{IM2H}} = \omega_{\mathrm{IF2}} \\ \omega_{\mathrm{IM2L}} - (\omega_{\mathrm{LO1}} - \omega_{\mathrm{LO2}}) = (\omega_{\mathrm{LO1}} - \omega_{\mathrm{LO2}}) - \omega_{\mathrm{RFL}} = \omega_{\mathrm{IF2}} \\ \omega_{\mathrm{IF1}} = \omega_{\mathrm{LO2}} + \omega_{\mathrm{IF2}} \end{cases} \tag{20}$$

where the suffix H and L represent high- and low-frequency operation modes, respectively.

For the first conversion, the positive spectrum of the desired signal (ω_{RFH}) is left-shifted to ω_{IF1} at the high-frequency mode, while the negative spectrum of the desired signal ($-\omega_{\mathrm{RFL}}$) is right-shifted to the same band (ω_{IF1}) at the low-frequency mode, as described in (20). Similar to the single-band case, the first image signal is shifted away from the output passband, while the second image signal is filtered out by the following multistage PPF in the Weaver–Hartley hybrid system. Note that this dual-band architecture cannot be realized by a conventional double-quadrature–double-quadrature topology because the double-quadrature–double-quadrature receiver pre-filters out the negative RF signal, which is our desired signal for the low-frequency operation mode; however, a dual-band double-quadrature–double-quadrature Weaver–Hartley receiver will be proposed in Section V.

B. Nonideal Effects

Input I/Q signal mismatch and device mismatch of the mixers are unavoidable for a practical circuit fabrication and lead to a degradation of the IRR. The device mismatch can be referred to an input I/Q signal gain/phase mismatch. When a quadrature phase error or an amplitude mismatch exists, opposite phasor sequence (or opposite complex-frequency signal) is induced, as described in Section II-A. Imperfect input signals can be represented as a positive spectrum with an error negative spectrum

$$e^{j\omega_1 t} + \varepsilon_1 e^{-j\omega_1 t} \tag{21a}$$

where $(\omega_1, \varepsilon_1) \in \{(\omega_{\mathrm{RF}}, \varepsilon_{\mathrm{RF}}), (\omega_{\mathrm{IM1}}, \varepsilon_{\mathrm{IM1}}), (\omega_{\mathrm{IM2}}, \varepsilon_{\mathrm{IM2}})\}$; $\varepsilon_{\mathrm{RF}}$, $\varepsilon_{\mathrm{IM1}}$, and $\varepsilon_{\mathrm{IM2}}$ are the input error functions at ω_{RF}, ω_{IM1}, and ω_{IM2}, respectively.

Similarly, imperfect quadrature LO_1 and LO_2 signals can also be decomposed into

$$e^{-j\omega_{\mathrm{LO1}}t} + \varepsilon_{\mathrm{LO1}} e^{j\omega_{\mathrm{LO1}}t} \tag{21b}$$

$$e^{-j\omega_{\mathrm{LO2}}t} + \varepsilon_{\mathrm{LO2}} e^{j\omega_{\mathrm{LO2}}t}. \tag{21c}$$

All of the error functions are much smaller than unity. Note that, for the low-band operation of the dual-band architecture, the LO_1 signal should be switched to $e^{j\omega_{\mathrm{LO1}}t} + \varepsilon'_{\mathrm{LO1}} e^{-j\omega_{\mathrm{LO1}}t}$, as shown in Fig. 6(b).

After the complex mixing operation at the first stage, as shown in Fig. 6(a), we can obtain

$$e^{j(\omega_1 - \omega_{\mathrm{LO1}})t} + \varepsilon_1 \varepsilon_{\mathrm{LO1}} e^{-j(\omega_1 - \omega_{\mathrm{LO1}})t}. \tag{21d}$$

Here, the high-frequency terms are negligible thanks to the inherent low-pass characteristics of active mixers.

By the same token, the outputs after the second conversion can be expressed as follows:

$$\begin{cases} e^{j\omega_{\mathrm{IF2}}t} + \varepsilon_{\mathrm{PPF(IF2)}} \varepsilon_{\mathrm{RF}} \varepsilon_{\mathrm{LO1}} \varepsilon_{\mathrm{LO2}} e^{-j\omega_{\mathrm{IF2}}t} \ (\mathrm{RF\ input}) \\ \varepsilon_{\mathrm{IM1}} \varepsilon_{\mathrm{LO1}} e^{j\omega_{\mathrm{IF2}}t} + \varepsilon_{\mathrm{PPF(IF2)}} \varepsilon_{\mathrm{LO2}} e^{-j\omega_{\mathrm{IF2}}t} \ (\mathrm{IM}_1\ \mathrm{input}) \\ \varepsilon_{\mathrm{IM2}} \varepsilon_{\mathrm{LO1}} \varepsilon_{\mathrm{LO2}} e^{j\omega_{\mathrm{IF2}}t} + \varepsilon_{\mathrm{PPF(IF2)}} e^{-j\omega_{\mathrm{IF2}}t} \ (\mathrm{IM}_2\ \mathrm{input}) \end{cases} \tag{21e}$$

where $\varepsilon_{\mathrm{PPF(IF2)}}$ is the error function of the PPF at the output of the second-stage mixers.

Similar to a double-quadrature–double-quadrature down-converter, a single-quadrature–double-quadrature down-converter with differential input signals can be treated as a complex mixing with the input error function ε_1, defined in (21a), equaling 1. The IF outputs of a single-quadrature–double-quadrature down-converter are directly rewritten as

$$\begin{cases} e^{j\omega_{\mathrm{IF2}}t} + \varepsilon_{\mathrm{PPF(IF2)}} \varepsilon_{\mathrm{LO1}} \varepsilon_{\mathrm{LO2}} e^{-j\omega_{\mathrm{IF2}}t} \ (\mathrm{RF\ input}) \\ \varepsilon_{\mathrm{LO1}} e^{j\omega_{\mathrm{IF2}}t} + \varepsilon_{\mathrm{PPF(IF2)}} \varepsilon_{\mathrm{LO2}} e^{-j\omega_{\mathrm{IF2}}t} \ (\mathrm{IM}_1\ \mathrm{input}) \\ \varepsilon_{\mathrm{LO1}} \varepsilon_{\mathrm{LO2}} e^{j\omega_{\mathrm{IF2}}t} + \varepsilon_{\mathrm{PPF(IF2)}} e^{-j\omega_{\mathrm{IF2}}t} \ (\mathrm{IM}_2\ \mathrm{input}). \end{cases} \tag{21f}$$

Equations (21e) and (21f) provide detailed information for IRR degradation. Compared with (21e) and (21f), the IRR_1 of a double quadrature system is $\varepsilon_{\mathrm{IM1}}^{-1}$ times larger than that of a single-quadrature system; thus, a fully double-quadrature

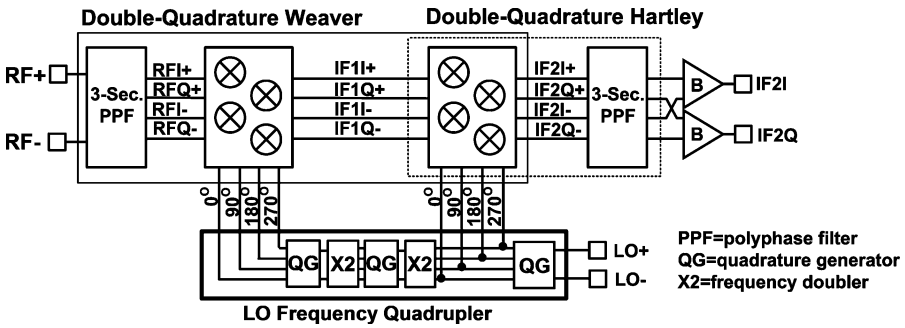

Fig. 7. Block diagram of a 0.35-μm SiGe HBT double-quadrature–double-quadrature Weaver–Hartley low-IF downconverter.

system typically provides a higher IRR. However, if the quadrature LO signals are not accurate enough, the IRR_2 still degrades, but a double-quadrature–double-quadrature system suppresses the effect of the LO quadrature accuracy by a factor of $\varepsilon_{\mathrm{IM2}}^{-1}$, and thus guarantees that the IRR_2 can be almost determined by the IF_2 PPF. To solve the drawback of a single-quadrature–double-quadrature topology, an inter-stage PPF centered at ω_{IF1} with a frequency response of $\varepsilon_{\mathrm{PPF(IF1)}}$ is inserted between the first- and second-stage mixers, as shown in Fig. 6(b). The outputs of the modified dual-conversion system are described as follows:

$$\begin{cases} e^{j\omega_{\mathrm{IF2}}t}+\varepsilon_{\mathrm{PPF(IF2)}}\varepsilon_{\mathrm{LO2}}\varepsilon_{\mathrm{PPF(IF1)}}\varepsilon_{\mathrm{LO1}}e^{-j\omega_{\mathrm{IF2}}t} \\ \quad (\mathrm{RF\ input}) \\ om_{\mathrm{LO1}}e^{j\omega_{\mathrm{IF2}}t}+\varepsilon_{\mathrm{PPF(IF2)}}\varepsilon_{\mathrm{LO2}}\varepsilon_{\mathrm{PPF(IF1)}}e^{-j\omega_{\mathrm{IF2}}t} \\ \quad (\mathrm{IM}_1\ \mathrm{input}) \\ \varepsilon_{\mathrm{PPF(IF1)}}\varepsilon_{\mathrm{LO1}}\varepsilon_{\mathrm{LO2}}e^{j\omega_{\mathrm{IF2}}t}+\varepsilon_{\mathrm{PPF(IF2)}}e^{-j\omega_{\mathrm{IF2}}t} \\ \quad (\mathrm{IM}_2\ \mathrm{input}). \end{cases} \tag{21g}$$

The inserted inter-stage PPF guarantees a higher system dynamic range by reducing the large first image signal before entering the second-stage mixers even though IRR_1 cannot be improved [9]. However, when compared with (21f) and (21g), the quadrature accuracy of the IF signal is further improved and IRR_2 can be further pushed to the theoretical limit of the IF_2 PPF.

IV. Circuit Design and Measurement Results

A. 5.2-GHz Double-Quadrature–Double-Quadrature Dual-Conversion Low-IF Downconverter

Fig. 7 shows the block diagram of a 0.35-μm SiGe HBT double-quadrature–double-quadrature dual-conversion low-IF downconverter and corresponds to the architecture in Fig. 6(a). In a double-quadrature–double-quadrature downconverter, both the first- and second-stage complex mixers contain four Gilbert mixers.

Correlated LO signals (LO_1 and LO_2) with the same phase error maintain a maximum IRR [12]. Fig. 8(a) and (b) shows the mathematical expression and the schematic of the compensated frequency doubler [20]; thus, the self-mixing dc offset, generated by the current phase delay (θ), can be eliminated. The LO frequency quadrupler in Fig. 7 consists of two compensated frequency doublers to generate coherent signals with less phase error.

A three-stage PPF is employed at the RF port for a quadrature signal generation at three bands f_{RF}, f_{IM1}, and f_{IM2}. Since

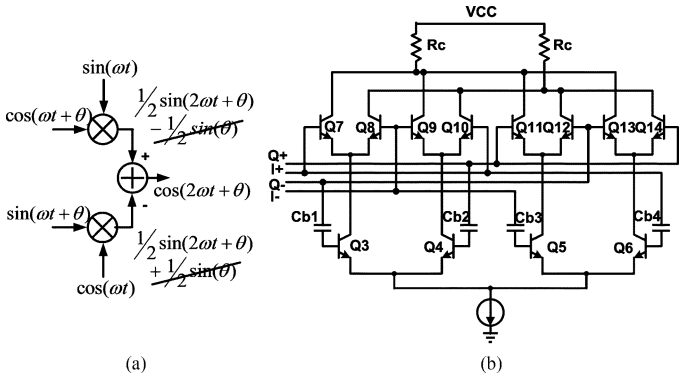

Fig. 8. (a) Block diagram of a high-precision compensated frequency doubler. (b) Schematic of the compensated frequency doubler employed in the LO quadrupler (bias circuit is not shown for simplicity).

f_{RF} (5.2 GHz) $> f_{\mathrm{IM2}}$ (5.14 GHz) $> f_{\mathrm{IM1}}$ (3.072 GHz), the transmission zeros of the three stages are set according to this order to minimize the loss of PPF. Therefore, the desired signal and image signals are perfectly quadrature in nature.

In the LO quadruplers, two-stage PPFs are employed in the $\mathrm{LO}_1/\mathrm{LO}_2$ output quadrature generators and the quadrature generator required by the compensated frequency doublers, as shown in Fig. 8. The center frequencies of the two-stage PPFs are set the same and the resistance in the second stage is twice as large as that in the first stage while the capacitance is only half. Since the unlicensed national information infrastructure (U-NII) band is covering 5.15–5.35 GHz with 200 MHz bandwidth, it means a ratio bandwidth of $1.04(=5.35/5.15)$ for the RF band is needed. However, the implemented signal bandwidth needs to be designed wider than the required one to tolerate the silicon process variation. As described in Section II-B, the IRR at the original center frequency becomes 20.8 dB for a single-stage PPF and 41.6 dB for a two-stage PPF if a 20% frequency deviation is applied. Therefore, a two-stage cascade PPF is sufficient for the LO generator when considering both the required signal bandwidth and process variation if a 40-dB IRR is set as the criterion. Besides, in order to obtain about 50-dB IRR within the bandwidth of 15–35 MHz, a three-stage PPF is incorporated at the end of the downconverter.

A die photograph of the 5.2-GHz downconverter is shown in Fig. 9 and the die size is 1.6×1.35 mm^2. The total current of eight mixers is 32 mA at a 3.3-V supply, while the LO generator and the IF output buffers consume 35 mA. A conversion gain reaches 10 dB when the LO power is larger than -4 dBm. The measured single-sideband noise figure (SSB-NF) is lower than

TABLE I
PERFORMANCE COMPARISONS

Reference		[7]	[8]		[9]	[10]		This Work A	This Work B	
Topology (SQ=single-quadrature DQ=double-quadrature)		SQDQ Weaver	Dual-band SQDQ Weaver		SQDQ Weaver-Hartley	Dual-band SQDQ Weaver-Hartley		DQDQ Weaver-Hartley	Dual-band SQDQ Weaver-Hartley	
Supply Voltage (V)		3.3	3		3.3	1.8		3.3	1.8	
Power Consumption (mW)		198 [a]	75		115.5	126 (mixer:25)		210 (mixer:105)	95	
Frequency (GHz)		1.9	0.9	1.8	2.4	2.4	5.7	5.2	2.2	4.8
Conversion gain (dB)		26~78	23(A_V)	23(A_V)	20.3 (max)	9	8	10	14.2	12.7
Noise figure (dB)		14 (min)	4.7	4.9	7.2 (min)	23	25	18	6.2	7.2
IRR_1 (dB)	Rx	55	40	36	35	N.A.	N.A.	N.A.	56	52
	Rx w/o LNA	45	N.A.	N.A.	N.A.	40	40	55	49.5	37
IRR_2 (dB)		N.A. [b]	N.A. [b]	N.A. [b]	60 [c]	44	46	50	77	74
Technology		0.6-μm CMOS	0.6-μm CMOS		0.6-μm CMOS	0.18-μm CMOS		0.35-μm SiGe HBT	0.18-μm CMOS	

[a]Including ADC and baseband filter.
[b]IF_2=0.
[c]5-stage polyphase filter and passive IF mixers.

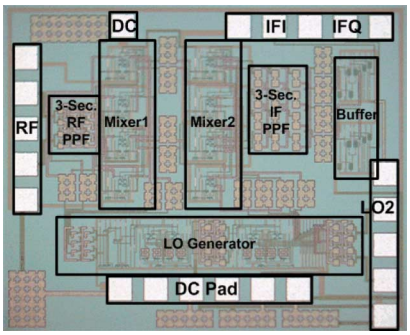

Fig. 9. Die photograph of the 0.35-μm SiGe HBT double-quadrature–double-quadrature Weaver–Hartley low-IF downconverter.

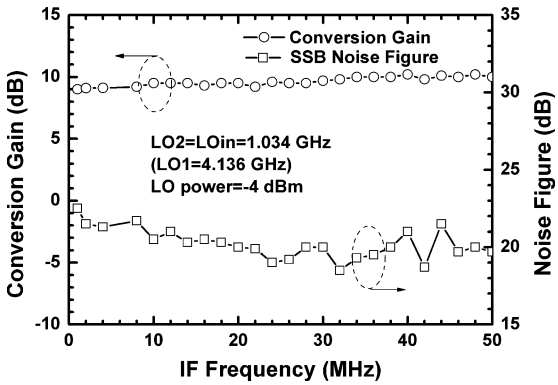

Fig. 10. Conversion gain and SSB-NF of the 0.35-μm SiGe HBT double-quadrature–double-quadrature Weaver–Hartley low-IF down-converter.

20 dB for f_{IF2} ranging from 15 to 35 MHz, as shown in Fig. 10. The flicker noise corner in Fig. 10 is absent (less than 1 MHz) thanks to the low flicker noise of SiGe HBT devices. The downconverter has an $\mathrm{IP}_{1\mathrm{dB}}$ of -8 dBm and an IIP_3 of 9 dBm when $f_{\mathrm{RF}} = 5.2$ GHz, $f_{\mathrm{LO2}} = 1.034$ GHz, $f_{\mathrm{LO1}} = 4 \times f_{\mathrm{LO2}}$, and $f_{IF} = 30$ MHz. Fig. 11 shows the IRR from three samples to be on average about 55/50 dB for the first/second image signals, respectively. The IRR of the second image signal has a bandpass shape because the PPF is a complex notch filter for the negative spectrum covering 15–35 MHz, while the frequency response of

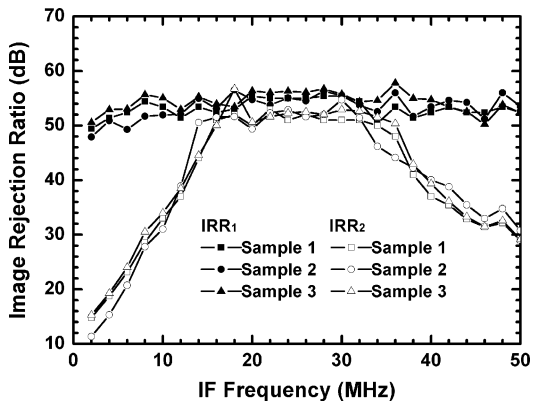

Fig. 11. IRR for the first/second image signals in three samples of the 0.35-μm SiGe HBT double-quadrature–double-quadrature Weaver–Hartley low-IF downconverter.

the positive spectrum is relatively flat [10]. The LO-to-RF isolation is 52 dB. The measured performance is summarized and compared with state-of-the-art architectures in Table I.

B. 2.2/4.8-GHz Single-Quadrature–Double-Quadrature Dual-Conversion Low-IF Downconverter

Fig. 12 shows the block diagram of a 0.18-μm CMOS single-quadrature–double-quadrature dual-band low-IF receiver consisting of a dual-band LNA, a single-quadrature Hartley system and a double-quadrature Hartley system. Moreover, the cascaded complex mixer topology corresponding to the architecture in Fig. 6(b) can be treated as a Weaver architecture. Fig. 13(a) shows that the switched-band LNA consists of a switchable notch filter in the second stage. Previously, a notch filter consisting of a series LC resonator was inserted in the LNA to provide an additional IRR and suppress interference [21], [22]. In this work, a switchable notch filter is employed. The resonance frequency is $1/\sqrt{L(C_1+C_2)}$ or $1/\sqrt{LC_1}$ when the control transistor is on or off, respectively. The simulated frequency response of the switched-band LNA with and without a switchable notch filter is shown in Fig. 13(b). The IRR_1 of a single-quadrature–double-quadrature downconverter

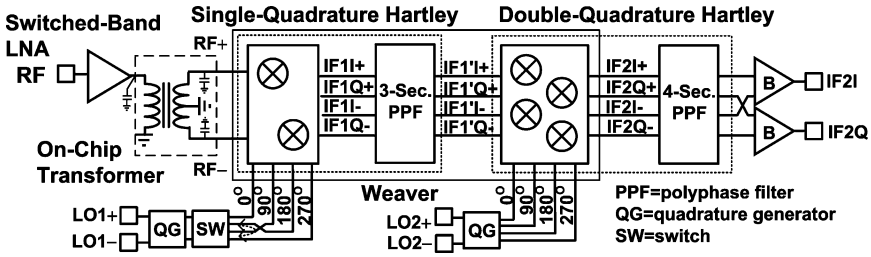

Fig. 12. Block diagram of a dual-band 0.18-μm CMOS single-quadrature–double-quadrature Weaver–Hartley low-IF downconverter.

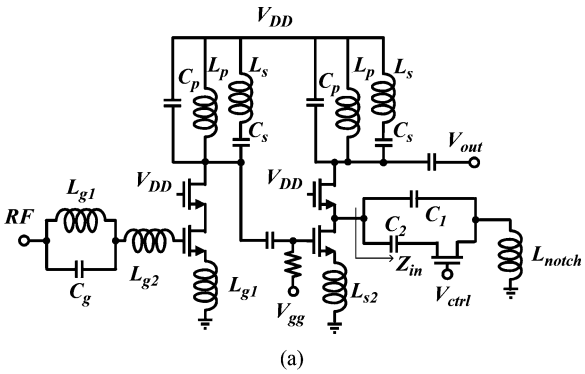

(a)

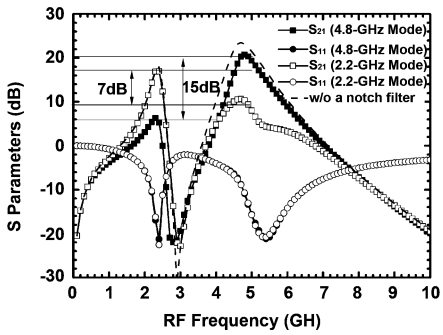

(b)

Fig. 13. (a) Schematic of the LNA with a switchable notch filter. (b) Simulated frequency response.

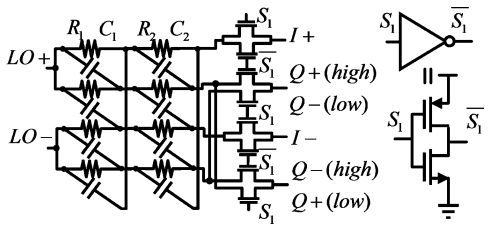

Fig. 14. LO_1 quadrature signal generator with a two-stage PPF and NMOS switch pairs.

can be improved by a preceding narrowband LNA to achieve over 50-dB IRR.

An on-chip miniature single-to-differential 3:2 transformer is utilized at the output of the LNA to generate differential RF signals compatible to the following double-balanced Gilbert mixers with a common-gate input stage.

As shown in Fig. 14, two-stage PPFs generate differential-quadrature LO signals, including first- and second-stage LO signals, from differential inputs. Moreover, four NMOS switch pairs are employed at the outputs of the LO_1 generator [10]. If the control bit is high or low, a 2.2- or 4.8-GHz band is thus selected, respectively. LO_1 is set at the halfway point between

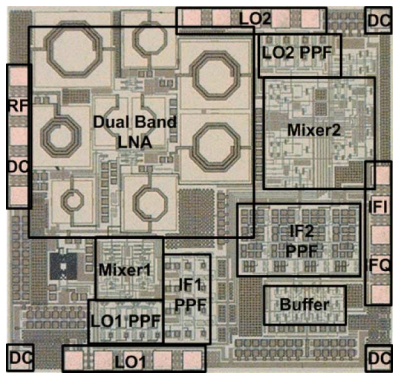

Fig. 15. Die photograph of the dual-band 0.18-μm CMOS single-quadrature–double-quadrature Weaver–Hartley low-IF downconverter.

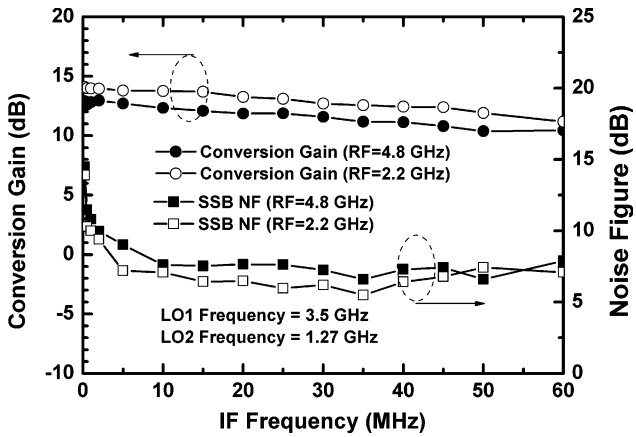

Fig. 16. Conversion gain and SSB-NF of the dual-band 0.18-μm CMOS single-quadrature–double-quadrature Weaver–Hartley low-IF downconverter.

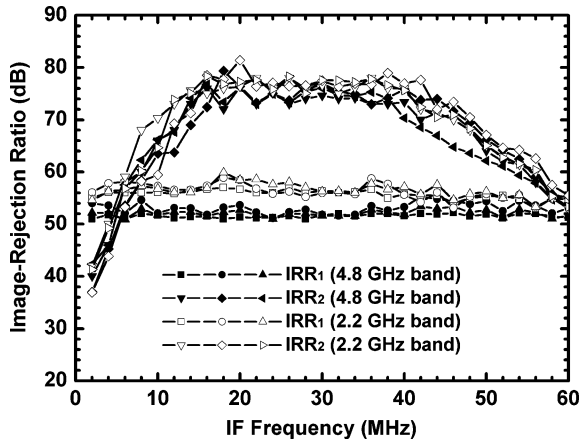

Fig. 17. IRR for the first/second image signals in three samples of the dual-band 0.18-μm CMOS single-quadrature–double-quadrature Weaver–Hartley low-IF downconverter.

two application bands (2.2 and 4.8 GHz) to reuse the first-stage mixers (i.e., LO_1 is around 3.5 GHz, and thus, LO_2 is around

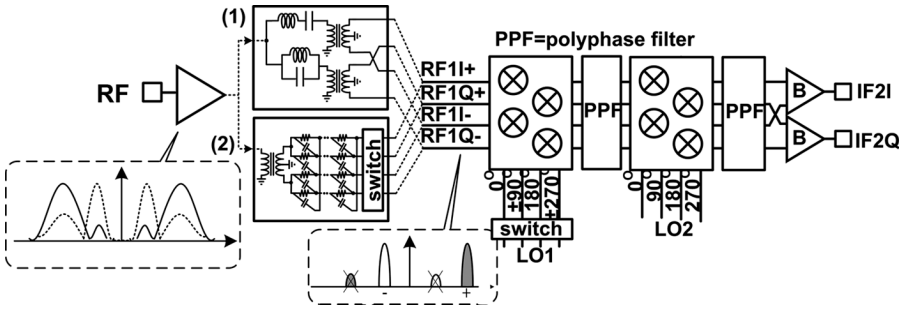

Fig. 18. Block diagram of a dual-band double-quadrature–double-quadrature dual-conversion low-IF downconverter.

1.27 GHz with IF_2 covering from 20 to 40 MHz). The frequency relations were introduced in (20).

The single-quadrature Hartley system, after the transformer, consists of two Gilbert mixers and a three-stage PPF, while the following double-quadrature Hartley system has four mixers and a four-stage PPF.

A three-stage inter-stage PPF has the ratio bandwidth of 1.4938 for a 60-dB IRR. A higher quality in quadrature input signals guarantees the maximum achievable IRR. On the other hand, the four-stage IF_2 PPF is designed for an 80-dB IRR covering 20–40 MHz (ratio bandwidth $= 2$).

A die photograph of the dual-band low-IF downconverter is shown in Fig. 15, and the die size is 1.83×1.94 mm^2. The total power consumption is 95 mW at a 1.8-V supply. The conversion gain and SSB-NF are shown in Fig. 16. The conversion gain is 14.2/12.7 dB with the in-band (20–40 MHz) SSB-NF of 6.2/7.2 dB at 2.2/4.8-GHz modes, respectively. Besides, the flicker noise corner of the demonstrated CMOS receiver for both modes is around 5 MHz, which is away from our IF band. $\mathrm{IP}_{1\mathrm{dB}}/\mathrm{IIP}_3$ is $-25/-10$ dBm at the 2.2-GHz mode, while $\mathrm{IP}_{1\,\mathrm{dB}}/\mathrm{IIP}_3$ becomes $-27/-16$ dBm at the 4.8-GHz mode when $\mathrm{LO}_1 = 3.5$ GHz, $\mathrm{LO}_2 = 1.27$ GHz, and $\mathrm{IF}_2 = 30$ MHz, respectively. Fig. 17 shows the IRR_1 and IRR_2 at 2.2/4.8-GHz modes from three samples. As shown in Fig. 17, IRR_1 is on average about 56/52 dB at the 2.2/4.8-GHz mode, while the IRR_2 is about 77/74 dB. The $\mathrm{LO}_1/\mathrm{LO}_2$-to-RF isolation reaches 77/71 dB. The input return loss is better than -10 dB within 2–2.5 and 4.6–5.7 GHz for both modes. The overall measured performance is also summarized in Table I.

V. Conclusion

The characteristics of a PPF with different locations of transmission zeros for single-band or multiband applications has been intensively discussed. A double-quadrature system with the preceding PPF has much immunity of quadrature amplitude/phase mismatch, and thus is preferred at both the first- and second-stage mixers to achieve excellent IRR at the cost of power consumption. Thus, a dual-conversion double-quadrature–double-quadrature low-IF downconverter with an input RF PPF and a dual-band dual-conversion single-quadrature–double-quadrature low-IF downconverter with an inter-stage PPF have been demonstrated in this paper for a significant improvement in image rejection. A double-quadrature–double-quadrature downconverter with an RF PPF in our work achieves a 55-dB IRR_1. On the other hand, the IRR_1 of a single-quadrature–double-quadrature downconverter without an LNA is less than 45 dB, as summarized in Table I. The dual-band single-quadrature–double-quadrature downconverter with an inserted inter-stage PPF in our work achieves 77/74 dB IRR_2 at 2.2/4.8-GHz and demonstrates the state-of-the-art IRR_2 in the literature, as summarized in Table I. The proposed two architectures can almost reach the theoretical limit of the IF_2 PPF.

Further, a dual-band double-quadrature–double-quadrature architecture has been proposed here for further image rejection improvements (both IRR_1 and IRR_2), as shown in Fig. 18. As mentioned in Section III-A, the proposed dual-band architecture requires opposite quadrature RF polarities at the two operating frequencies; thus a conventional double-quadrature–double-quadrature topology cannot be realized as a dual-band variant straightforwardly. A dual-band quadrature RF signal generation with opposite polarities can be achieved two ways, which are: 1) a dual-band LR-CR topology [23] and 2) a multistage PPF with different transmission zeros and followed by switch pairs, similar to the LO_1 switch pairs shown in Fig. 14. When operating at a high-frequency band, the polarity is positive, but the polarity is switched to be negative at a low-frequency operation mode. Moreover, a switched-band LNA is preferred since any interference (including the image signals) can be pre-filtered out by the LNA. Therefore, the proposed dual-band architecture maintains excellent image-rejection performance by the double-quadrature–double-quadrature topology and the inter-stage PPF.

References

[1] S. J. Fang, A. Bellaouar, S. T. Lee, and D. J. Allstot, "An image-rejection downconverter for low-IF receivers," *IEEE Trans. Microw. Theory Tech.*, vol. 53, no. 2, pp. 478–487, Feb. 2005.

[2] W. Kluge, F. Poegel, H. Roller, M. Lange, T. Ferchland, L. Dathe, and D. Eggert, "A fully integrated 2.4-GHz ieee 802.15.4-compliant transceiver for ZigBee™ applications," *IEEE J. Solid-State Circuits*, vol. 41, no. 12, pp. 2767–2775, Dec. 2006.

[3] I. Nam, K. Choi, J. Lee, H.-K. Cha, B.-I. Seo, K. Kwon, and K. Lee, "A 2.4 GHz low-power low-IF receiver and direct-conversion transmitter in 0.18-μm CMOS for IEEE 802.15.4 WPAN applications," *IEEE Trans. Microw. Theory Tech.*, vol. 55, no. 4, pp. 682–689, Apr. 2007.

[4] H. Darabi and A. A. Abidi, "Noise in RF-CMOS mixers: A simple physical model," *IEEE J. Solid-State Circuits*, vol. 35, no. 1, pp. 15–25, Jan. 2000.

[5] J. Yoon, H. Kim, C. Park, J. Yang, H. Song, S. Lee, and B. Kim, "A new RF CMOS Gilbert mixer with improved noise figure and linearity," *IEEE Trans. Microw. Theory Tech.*, vol. 56, no. 3, pp. 626–631, Mar. 2008.

[6] S. Zhou and M.-C. F. Chang, "A CMOS passive mixer with low flicker noise for low-power direct-conversion receiver," *IEEE J. Solid-State Circuits*, vol. 40, pp. 1084–1093, May 2005.

[7] J. C. Rudell, J.-J. Ou, T. B. Cho, G. Chien, F. Brianti, J. A. Weldon, and P. R. Gray, "A 1.9-GHz wide-band IF double conversion CMOS integrated receiver for cordless telephone applications," *IEEE J. Solid-State Circuits*, vol. 32, no. 12, pp. 2071–1088, Dec. 1997.

[8] S. Wu and B. Razavi, "A 900-MHz/1.8-GHz CMOS receiver for dual-band applications," *IEEE J. Solid-State Circuits*, vol. 33, no. 12, pp. 2178–2185, Dec. 1998.

[9] F. Behbahani, J. C. Leete, Y. Kishigami, A. Roithmeier, K. Hoshino, and A. A. Abidi, "A 2.4-GHz low-IF receiver for wideband WLAN in 0.6-μm CMOS-architecture and front-end," *IEEE J. Solid-State Circuits*, vol. 35, no. 12, pp. 1908–1908, Dec. 2000.

[10] C. C. Meng, T.-H. Wu, J.-S. Syu, S.-W. Yu, K.-C. Tsung, and Y.-H. Teng, "2.4/5.7-GHz CMOS dual-band low-IF architecture using Weaver–Hartley image-rejection techniques," *IEEE Trans. Microw. Theory Tech.*, vol. 57, no. 3, pp. 552–561, Mar. 2009.

[11] D. Weaver, "A third method of generation and detection of single-sideband signals," *Proc. IRE*, vol. 44, no. 12, pp. 1703–1705, Dec. 1956.

[12] T.-H. Wu and C. C. Meng, "5.2/5.7-GHz 48-dB image rejection GaInP/GaAs HBT Weaver downconverter using LO frequency quadrupler," *IEEE J. Solid-State Circuits*, vol. 41, no. 11, pp. 2468–2480, Nov. 2006.

[13] R. Hartley, "Modulation system," U.S. Patent 1 666 206, Apr. 17, 1928.

[14] H.-K. Chiou, W.-R. Lian, and T.-Y. Yang, "A miniature Q-band balanced sub-harmonically pumped image rejection mixer," *IEEE Microw. Wireless Compon. Lett.*, vol. 17, no. 6, pp. 463–465, Jun. 2007.

[15] F. Behbahani, Y. Kishigami, J. Leete, and A. A. Abidi, "CMOS mixers and polyphase filters for large image rejection," *IEEE J. Solid-State Circuits*, vol. 36, no. 6, pp. 873–887, Jun. 2001.

[16] J. Crols and M. Steyaert, "A single-chip 900 MHz CMOS receiver front-end with a high-performance low-IF topology," *IEEE J. Solid-State Circuits*, vol. 30, no. 12, pp. 1483–1492, Dec. 1995.

[17] S. Tadjpour, E. Cijvat, E. Hegazi, and A. A. Abidi, "A 900-MHz dual-conversion low-IF GSM receiver in 0.35-μm CMOS," *IEEE J. Solid-State Circuits*, vol. 36, no. 12, pp. 1992–2002, Dec. 2001.

[18] M. J. Gingell, "Single-sideband modulation using sequence asymmetric polyphase networks," *Elect. Commun.*, vol. 48, no. 1–2, pp. 21–25, 1973.

[19] B. Razavi, *RF Microelectronics*. Upper Saddle River, NJ: Prentice-Hall, 1998, pp. 138–142.

[20] A. W. Buchwald, K. W. Martin, A. K. Oki, and K. W. Kobayashi, "A 6-GHz integrated phase-locked loop using AlGaAs/GaAs heterojunction bipolar transistors," *IEEE J. Solid-State Circuits*, vol. 27, no. 12, pp. 1752–1762, Dec. 1992.

[21] H. Samavati, H. R. Rategh, and T. H. Lee, "A 5-GHz CMOS wireless lan receiver front end," *IEEE J. Solid-State Circuits*, vol. 35, no. 5, pp. 765–772, May 2000.

[22] T.-K. Nguyen, N.-J. Oh, C.-Y. Cha, Y.-H. Oh, G.-J. Ihm, and S.-G. Lee, "Image-rejection CMOS low-noise amplifier design optimization techniques," *IEEE Trans. Microw. Theory Tech.*, vol. 53, no. 2, pp. 538–546, Feb. 2005.

[23] S.-C. Tseng, C. C. Meng, and Y.-T. Lee, "Dual-band adjustable and reactive I/Q generator with constant resistance for down- and up-converters," *IEEE Trans. Microw. Theory Tech.*, vol. 56, no. 8, pp. 1861–1868, Aug. 2008.

Jin-Siang Syu (S'09) was born in Taoyuan, Taiwan, in 1984. He received the B.S. degree in communication engineering from National Chiao Tung University, Hsinchu, Taiwan, in 2006, and is currently working toward the Ph.D. degree in electrical engineering at National Chiao Tung University.

His current research interests are in the areas of RF integrated circuits (RFICs).

Mr. Syu is a member of Phi Tau Phi.

Chin-Chun Meng (M'02) received the B.S. degree in electrical engineering from National Taiwan University, Taipei, Taiwan, in 1985, and the Ph.D. degree in electrical engineering from the University of California at Los Angeles (UCLA), in 1992.

He is currently a Full Professor with the Department of Electrical Engineering, National Chiao Tung University (NCTU), Hsinchu, Taiwan. His current research interests are in the areas of RF integrated circuits (RFICs) and microwave and millimeter-wave integrated circuits.

Ya-Hui Teng was born in Pingtung, Taiwan, in 1983. She received the B.S. and M.S. degrees in communication engineering from National Chiao Tung University, Hsinchu, Taiwan, in 2006 and 2008, respectively. Her M.S. research concerned CMOS dual-band image-rejection receiver and ultra-wideband downconverters.

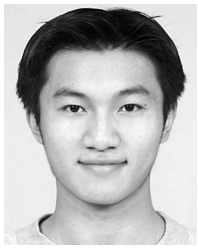

Hua-Yu Liao was born in Taipei, Taiwan, in 1982. He received the B.S. and M.S. degrees in communication engineering from National Chiao Tung University, Hsinchu, Taiwan, in 2004 and 2006, respectively. His M.S. research concerned SiGe HBT image-rejection down-converters and dual-band LNAs.